Article-citation info:
Remha S, Laouamer M, Mahmoudi A, Adika M, Soufi Y. A residual current-based indicator for early detection of stator winding faults in synchronous reluctance machines. Diagnostyka. 2026;27(1):2026109. https://doi.org/10.29354/diag/219271.

DIAGNOSTYKA, 2026, Vol. 27, No. 1

e-ISSN 2449-5220
DOI: 10.29354/diag/219271

A RESIDUAL CURRENT-BASED INDICATOR FOR EARLY DETECTION OF STATOR WINDING FAULTS IN SYNCHRONOUS RELUCTANCE MACHINES

Souhaib REMHA [1, 2, *], Mosbah LAOUAMER [1, 2], Abdelkader MAHMOUDI [1, 3], Mohamed ADIKA [4], Youcef SOUFI [5]

[1] Department of Mechanical Engineering, Faculty of Technology, University of El Oued, El Oued, 39000, Algeria
[2] UDERZA Unit, Faculty of Technology, University of El Oued, El Oued, 39000, Algeria
[3] CISE – Electromechatronic Systems Research Centre, University of Beira Interior, Covilhã, Portugal
[4] LPMRN Laboratory, Department of Electromechanical Engineering, University Mohamed El Bachir El Ibrahimi of Bordj Bou Arreridj, El-Anasser, Bordj Bou Arreridj, 34030, Algeria
[5] LABGET Laboratory, Department of Electrical Engineering, Faculty of Sciences and Technology, University of Tebessa, Tebessa, 12002, Algeria
[*] Corresponding author, e-mail: remha-souhaib@univ-eloued.dz

Abstract

The early identification of inter-turn short-circuit faults (ITSCFs) in electrical machines has become a priority due to their detrimental influence on reliability and efficiency. However, achieving accurate detection under closed-loop control remains challenging. Conventional second-harmonic-based methods are highly dependent on electromagnetic torque and machine parameters, reducing robustness. This study proposes a parameter-independent fault indicator for synchronous reluctance machines (SynRMs) based on the residual difference between measured and reference dq-axis currents. Simulation results demonstrate that the proposed indicator amplifies the fault-related second harmonic up to 0.47 p.u., compared to less than 0.01 p.u. in conventional dq products. Under both steady-state and transient conditions, the method successfully detects weak faults (μ = 4%) and severe faults (μ = 16%) with a short detection delay of approximately 0.038 s, while remaining insensitive to load torque variations up to 14 N·m and speed changes from 400 to 1500 rpm. The approach eliminates torque dependence and parameter sensitivity, providing a robust and computationally efficient framework suitable for real-time predictive maintenance applications.

Keywords: Synchronous Reluctance Machine (SynRM), Inter-Turn Short-Circuit Fault (ITSCF), harmonics, fault detection indicator

List of Symbols/Acronyms

AI – Artificial intelligence;
ANNs – Artificial Neural Networks;
FD – Fault Decision;
FEM – Finite Element Modeling;
FFT – Fast Fourier Transform;
HIL – Hardware-In-the-Loop;
IC – Incremental Counter;
IPMs – Permanent Magnet Motors;
ITSCFs – Inter-Turn Short-Circuit Faults;
MCSA – Motor Current Signature Analysis;
ML – Machine Learning;
PMSMs – Permanent Magnet Synchronous Machines;
STFT – Short-Time Fourier Transform;
SVMs – Support Vector Machines;
SynRMs – Synchronous Reluctance Machines;
WT – Wavelet Transform;
v_a, v_b, v_c – Phase voltages;
i_a, i_b, i_c – Stator currents;
R_s – Stator winding resistance;
L – Self-inductance of each phase;
M – Mutual inductance between stator windings;
L_{ls} – Leakage inductance;
L_A – Rotor position-independent inductance;
L_B – Rotor position-dependent inductance;
p – Number of pole pairs;
L_d, L_q – Direct/quadrature axis inductances;
i_d, i_q – dq-axis currents;
J – Moment of inertia;
ω_m – Mechanical speed;
B_m – Viscous friction coefficient;
T_L – Load torque;
T_f – Constant friction torque;
T – Period of the stator current;
Ts – Sampling time;
c – Sensitivity coefficient.

Received 2025-08-17; Accepted 2026-03-12; Available online 2026-03-17

1. INTRODUCTION

Recent progress in power electronics has significantly boosted the relevance of synchronous reluctance machines (SynRMs). These machines produce torque exclusively from the saliency produced by the variation in the direct (d) and quadrature (q) axis inductances, a feature made possible by their distinctive rotor design. In contrast to permanent magnet machines, SynRMs are immune to demagnetization issues, which translates into lower production costs, enhanced durability, and simpler rotor construction [1], [2]. These attributes have encouraged their adoption in diverse fields such as robotics, automotive traction, high-speed drives, and pumping systems [3]. Nonetheless, SynRMs still face challenges including low power factor, pronounced torque ripple, and acoustic noise [4], [5]. With their growing use in industry, the probability of unexpected failures has risen, leading to downtime, financial impact, and safety concerns. Among the most critical faults are inter-turn short circuits (ITSCFs) [6], [7].

The literature reports a broad spectrum of diagnostic strategies. Classical signal-based methods rely on spectral analysis tools such as FFT and STFT [8], or more advanced approaches including wavelet transforms, Hilbert-Huang techniques, and Wigner-Ville distributions [9]. Although artificial intelligence (AI) methods have shown promise [10]–[12], they typically require intensive computation and extensive training. Other techniques target specific harmonic distortions in current, voltage, or torque signals [13], [14], or use high-frequency signal injection [15]. Sensor-based solutions such as thermal monitoring [16], stray magnetic field mapping [17], and leakage flux measurement [18] add cost and complexity because of the need for external hardware. Meanwhile, model-based diagnostic schemes [19], [20] demand accurate knowledge of motor parameters, which may vary with operating conditions, reducing robustness.

Compared to permanent magnet synchronous and induction machines, SynRMs remain less investigated in the context of ITSCF detection. A few attempts exist, using methods such as artificial neural networks [21], hidden Markov models [22], odd-harmonic current analysis [23], and multi-sensor setups [24]. Research in this field has accelerated in line with the rising deployment of SynRMs [25]. While SynRMs are recognized for their eco-friendly and cost-effective design, they are also susceptible to a range of anomalies including inter-turn faults, eccentricity, and rotor misalignment [26]–[28]. Classical diagnostic techniques often exploit motor current signature analysis (MCSA) or FFT for fault feature extraction, and finite element modelling (FEM) is widely used to simulate such fault cases [29]. Still, when closed-loop controllers are present, early fault indicators are easily masked by feedback mechanisms or compensation signals [30].

To overcome these masking effects, researchers have begun leveraging AI and machine learning (ML). Models such as ANNs and SVMs have reported high detection accuracy under dynamic operating conditions [31]. Complementary approaches employ new indicators based on harmonic distortion, residual current analysis, or thermo-electromagnetic interactions [32]. Hybrid frameworks that integrate physical modelling, signal processing, and AI inference have recently emerged, offering adaptive and real-time detection suited to complex environments [33]. Nevertheless, the inherent robustness of closed-loop control introduces further complexity, since conventional open-loop fault detection techniques often fail when control feedback attenuates or conceals the fault signatures [35], [36]. Some studies suggest that control-related signals themselves may encode subtle fault information that can be exploited for early diagnosis.

From a critical review of current methodologies, five major limitations can be identified in adapting existing strategies to closed-loop SynRMs:

1. Heavy reliance on motor parameter accuracy.
2. Adverse influence of high-frequency signal injection on healthy operation.
3. Difficulty in extracting harmonic signatures from PI control loops [37].
4. Additional cost due to extra sensing devices.
5. Dependence on AI training datasets or lookup tables for classification [38].

The present work aims to design a computationally efficient, online detection scheme for ITSCFs in inverter-fed SynRMs under closed-loop control. The proposed approach introduces a fault indicator derived from torque equations, based on the residual between reference and measured dq-axis currents. This indicator demonstrates reduced sensitivity to load variations, while selective filtering of unwanted frequency components allows the enhancement of second-harmonic features. In this way, the method strengthens both the sensitivity and reliability of detection.

The remainder of this paper is organized as follows. Section II presents the mathematical modelling of the Synchronous Reluctance Machine (SynRM) under both healthy and faulty operating conditions. Section III details the architecture and design principles of the proposed fault detection scheme. Section IV provides simulation-based validation of the method, considering both steady-state and transient scenarios. Finally, Section V concludes the paper by summarizing the main findings and contributions.

2. SYNCHRONOUS RELUCTANCE MACHINE MODEL

This section presents the mathematical formulation of the SynRM under both healthy and inter-turn short-circuit fault (ITSCF) conditions. The

derived models were implemented and validated in MATLAB/Simulink.

2.1. Healthy SynRM Model in the abc Frame

The three-phase stator voltage equations in the stationary reference frame, aligned with the stator a, b, and c axes, can be expressed as:

$$\begin{bmatrix} v_a \\ v_b \\ v_c \end{bmatrix} = \begin{bmatrix} R_s & 0 & 0 \\ 0 & R_s & 0 \\ 0 & 0 & R_s \end{bmatrix} \begin{bmatrix} i_a \\ i_b \\ i_c \end{bmatrix} + \begin{bmatrix} L & M & M \\ M & L & M \\ M & M & L \end{bmatrix} \frac{d}{dt} \begin{bmatrix} i_a \\ i_b \\ i_c \end{bmatrix} \quad (1)$$

Assuming sinusoidally distributed stator windings, the self and mutual-inductance terms are:

$$\begin{cases} L = L_{1s} + L_A + L_B \\ M = -\frac{1}{2} L_A + L_B \end{cases} \quad (2)$$

The electromagnetic torque is:

$$T_e = \frac{3}{2}\, p\, (L_d - L_q)\, i_d\, i_q \quad (3)$$

If the direct-axis current i_d is held constant, (3) simplifies to:

$$T_e = K i_q \quad ; where: \; K = \frac{3}{2}\, p\, (L_d - L_q)\, i_d \quad (4)$$

The mechanical dynamic equation is:

$$T_e = J \frac{d\omega_m}{dt} + B_m \omega_m + T_L + T_k \quad (5)$$

where the rotor speed and position are related by:

$$\omega_e = p\omega_m \quad ; \quad \theta_e = \int \omega_e \, dt = 2p\theta_m \quad (6)$$

2.2. Faulty Model in the abc Frame

When an ITSCF occurs in phase aaa, let N represent the total turns of the phase and n the number of shorted turns. The ratio is $\mu=n/N$. The shorted portion carries current i_f through fault resistance R_f. As $R_f \to 0$, the condition approaches a complete short circuit.

Fig. 1 illustrates the equivalent circuit of a SynRM with an ITSCF in phase *a*. The presence of the fault causes magnetic asymmetry, leading to reduced performance and possible progression to more severe faults such as inter-phase short circuits.

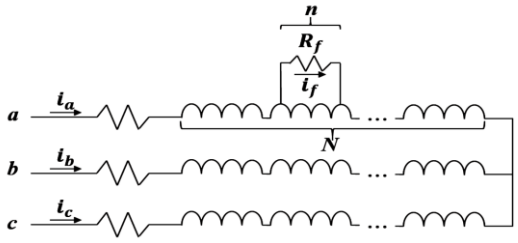

Fig. 1. Equivalent circuit of a series-connected synchronous reluctance machine (SynRM) exhibiting an inter-turn short-circuit fault in phase a

The voltage equations under this condition are:

$$\begin{bmatrix} v_a \\ v_b \\ v_c \\ v_f \end{bmatrix} = \begin{bmatrix} R_s & 0 & 0 & -uR_s \\ 0 & R_s & 0 & 0 \\ 0 & 0 & R_s & 0 \\ uR_s & 0 & 0 & -uR_s - R_f \end{bmatrix} \begin{bmatrix} i_a \\ i_b \\ i_c \\ i_f \end{bmatrix} + \begin{bmatrix} \mathrm{L} & \mathrm{M} & \mathrm{M} & -\mathrm{uL} \\ \mathrm{M} & \mathrm{L} & \mathrm{M} & -\mathrm{uM} \\ \mathrm{M} & \mathrm{M} & \mathrm{L} & -\mathrm{uM} \\ -\mathrm{uL} & \mathrm{uM} & \mathrm{uM} & -\mathrm{u^2L} \end{bmatrix} \frac{\mathrm{d}}{\mathrm{dt}} \begin{bmatrix} \mathrm{i_a} \\ \mathrm{i_b} \\ \mathrm{i_c} \\ \mathrm{i_f} \end{bmatrix} \quad (7)$$

2.3. Faulty SynRM Model in dq0 Frame

Applying Park's transformation to Equation (7) yields the dq0 representation:

$$\begin{cases} v_d = R_s i_d + L_d \frac{di_d}{dt} - \omega_e L_q i_q + \Delta v_{df} \\ v_d = R_s i_d + L_d \frac{di_d}{dt} - \omega_e L_q i_q + \Delta v_{df} \end{cases} \quad (8)$$

where the additional fault-induced voltage terms are:

$$\begin{cases} \Delta v_{df} = -\frac{2}{3} u R_s i_f \cos\theta - \frac{2}{3} u L_d \cos\theta \frac{di_f}{dt} + \\ \qquad \frac{2}{3} u \omega_e i_f (L_d - L_q) \sin\theta \\ \Delta v_{qf} = \frac{2}{3} u R_s i_f \sin\theta + \frac{2}{3} u L_q \sin\theta \frac{di_f}{dt} + \\ \qquad \frac{2}{3} u \omega_e i_f (L_d \sin\theta - L_q \cos\theta) \end{cases}$$

Equation (8) can be reformulated as:

$$\begin{cases} v_d = R_s i_{df} + L_d \frac{di_{df}}{dt} - \omega_e L_q i_{qf} \\ v_q = R_s i_{qf} + L_q \frac{di_{qf}}{dt} + \omega_e L_d i_{df} \end{cases} \quad (9)$$

with modified dq currents:

$$\begin{cases} \mathrm{i_{df}} = \mathrm{i_d} - \frac{2}{3} \mathrm{u i_f} \cos\theta \\ \mathrm{i_{qf}} = \mathrm{i_q} + \frac{2}{3} \mathrm{u i_f} \sin\theta \end{cases}$$

The inductances are given by:

$$L_{dq} = P L_s P^{-1} = diag\{L_d \quad L_q \quad L_{1s}\}$$
$$\begin{cases} \mathrm{L_d} = \mathrm{L_{1s}} + \frac{3}{2}(\mathrm{L_A} + \mathrm{L_B}) \\ \mathrm{L_q} = \mathrm{L_{1s}} + \frac{3}{2}(\mathrm{L_A} - \mathrm{L_B}) \end{cases} \quad (10)$$

3. PROPOSED DIAGNOSIS METHOD

This section is divided into two parts: a theoretical analysis of the fault signal and the design of the proposed detection method. The suggested technique is based on the electromagnetic torque equations of the SynRM to identify ITSCFs. The method operates within a closed-loop control system and does not rely on external sensors or high-frequency signal injection. It is implemented in a dynamic simulation model capable of injecting ITSC faults into any phase winding of the SynRM.

3.1. Fault Signal Analysis

SynRMs require precise control of multiple electrical variables [39]. Among these, electromagnetic torque is a key indicator since it incorporates both *d*- and *q*-axis current components. However, under non-stationary conditions or with varying load torque, torque-based detection becomes unreliable. Moreover, torque measurement often requires external sensors, limiting practicality.

To overcome this, the reference electromagnetic torque (from Equation (4)) is treated as the healthy torque signal, as it is largely unaffected by inter-turn faults. The actual electromagnetic torque under a fault, denoted as $T_{e,f}$, can be compared to the healthy reference torque $T_{e,h}$. The difference yields torque ripples, which carry valuable diagnostic information:

- Odd harmonics typically indicate rotor-related faults.

- Even harmonics are characteristic of ITSC faults.

The torque equation under fault conditions becomes:

$$T_{e,f} = T_{e,h} + T_{ripples} \quad (11)$$

$$T_{ripples} = \underbrace{\frac{3}{2}p\left(L_d - L_q\right)}_{K}\left(i_{df}i_{qf} - i_{dref}i_{qref}\right) \quad (12)$$

with : $i_d \approx i_{dref}, i_q \approx i_{qref}$

The multiplication of d- and q-axis currents enhances the visibility of ITSCFs, making even minor turn faults more detectable. This approach also inherently eliminates irrelevant components associated with the stationary abc frame, thereby isolating fault-relevant dynamics more effectively. As a result, the diagnostic term introduced in Equation (13) directly reflects the presence and impact of ITSCFs.

$$T_{ripples} = K\begin{pmatrix} -\frac{2}{3}u^2{i_f}^2\frac{sin^2(2\theta)}{2} + \\ \frac{2}{3}ui_f\left(i_d\,sin(\theta) - i_q\,cos(\theta)\right) \end{pmatrix} \quad (13)$$

To ensure that the fault indicator remains robust against variations in model parameters, the constant gain factor k used in the torque equation is deliberately excluded from the analysis. By removing this dependency, the proposed ITSCF indicator becomes independent of the machine's torque estimation process, as discussed in [40]. The indicator is instead derived from the comparison between measured and reference dq-axis currents:

$$\varepsilon = \mathrm{i_{df}}\cdot\mathrm{i_{qf}} - \mathrm{i_{dref}}\cdot\mathrm{i_{qref}}$$

$$\boldsymbol{\varepsilon} = \frac{1}{3}u^2{i_f}^2\,sin(2\theta)^2 + \frac{2}{3}ui_f\left(i_d\,sin(\theta) - i_q\,cos(\theta)\right) \quad (14)$$

While the second term in Equation (14) may be slightly influenced by changes in load torque, the first term is directly proportional to the fault severity and is thus more dominant. It should be emphasized that the fault current i_f and the fault ratio μ cannot be directly observed in practice, but their effects are captured in the measured dq currents. Therefore, this signal serves as a reliable and sensitive indicator for detecting ITSCFs, even in real-time applications.

3.2. Fault Detection Method Design

The proposed detection process is based on analysing the instantaneous variation in the second harmonic component of a residual between the measured and reference dq-axis currents in a closed-loop SynRM.

3.2.1. Dealing with Inherent Asymmetries

Due to practical issues such as manufacturing tolerances, current sensor limitations, inverter mismatch, and inherent magnetic imbalance [41], second harmonic components may appear even in healthy machines. Also, DC offsets are present in both healthy and faulty states.

To address this, the DC component is removed from both the measured and reference signals, aligning their average values. This operation is illustrated in Fig. 2, where mean value subtraction normalizes the signals, thereby enhancing fault visibility and minimizing sensitivity to transients.

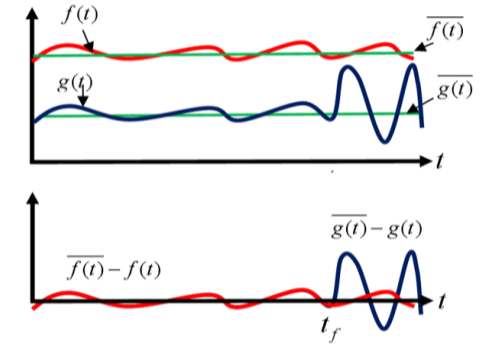

Fig. 2. Elimination of DC Component

3.2.2. Noise and Harmonics Filtering

Sensor noise and inverter switching frequency introduce additional distortions in the dq currents. To enhance the sensitivity of ε from (14), the signal is modulated by $cos(2\theta)$ and $sin(2\theta)$, and passed through a low–pass filter, as exposed in Fig. 3.

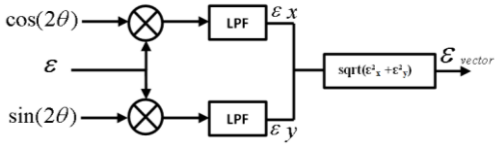

Fig. 3. Signal isolation of other harmonics

This step isolates the second harmonic while filtering out higher-order harmonics and noise-induced variations.

3.2.3. Speed Adaptation and Normalization

To maintain the fault indicator's effectiveness across varying operating speeds, the output signal is normalized through an averaging process. Specifically, the isolation vector derived from the measured and reference dq-axis current disparity is averaged over one full cycle. This average is then used as a base reference value, and the second harmonic component is expressed in per unit (p.u.) with respect to it.

$$|\varepsilon_{vector}|_N = \frac{|\overline{\varepsilon_{vector}}|}{\|\varepsilon_{vector}\|}[pu] \quad (15)$$

This normalized second harmonic, denoted as I_2, is given by:

$$I_2 = \frac{Extracted\ Second\ Harmonic}{Average\ Magnitude\ of\ the\ Isolation\ Vector} \quad (16)$$

The extracted harmonic is compared against a predefined threshold derived from healthy SynRM operation. Although second harmonic components can exist in the absence of faults due to inherent machine asymmetries and inverter imperfections, the magnitude increases significantly when an ITSCF occurs. Moreover, this component has low sensitivity to load torque variations, making it a robust fault indicator. However, abrupt changes in load can still cause slight disturbances, which must be accounted for in the detection logic.

3.2.3. False Alarm Prevention – Counting Algorithm

To mitigate false alarms caused by transient disturbances or abrupt system changes, a counting-based decision algorithm is introduced. This mechanism ensures that only persistent fault signatures are classified as true faults.

When the normalized fault signal I_2 exceeds the detection threshold, the algorithm activates an IC. This counter tracks how long the fault condition remains continuously active. If the condition is interrupted before reaching a minimum duration, the counter resets to zero, avoiding premature fault declarations.

The minimum required duration defined as COUNT is calculated by:

$$Count = \frac{T}{T_S} . c \tag{17}$$

A high c may delay detection or prevent it altogether. A low c may lead to spurious detections.

The FD is made based on the following logic:

$$FD = \begin{cases} 1 & , if \ IC \geq count \\ 0 & , \quad otherwise \end{cases} \tag{18}$$

This logic ensures that only stable, sustained anomalies trigger an alarm, significantly improving detection reliability in practical, noisy environments.

3.3. Diagnostic Flowchart

The complete flowchart of signal processing and fault detection from signal acquisition to decision logic is revealed in Fig. 4 (upper and lower sections).

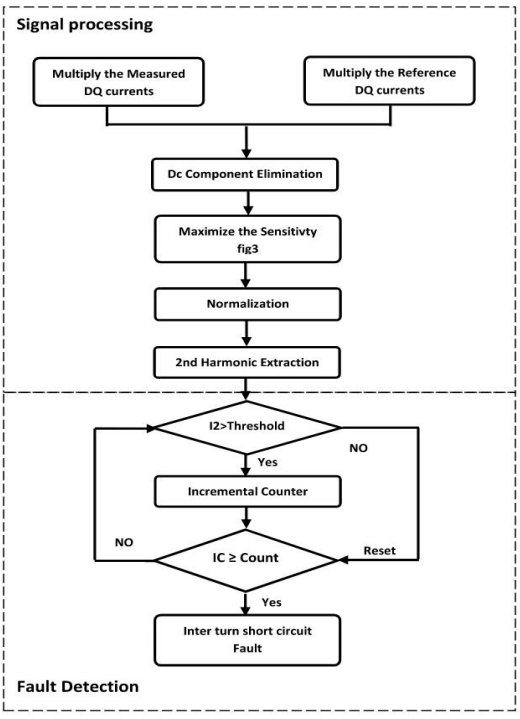

Fig. 4. Fault Detection Flowchart

4. SIMULATION RESULTS

The effectiveness of the proposed ITSCF detection method was evaluated through detailed simulations implemented in MATLAB/Simulink environment. The diagnostic technique was applied to SynRM stator Fault Model as defined in Section 2.2. Table 1 summarizes the key machine parameters used during the simulation.

The SynRM is supplied by a three-phase voltage source inverter (VSI) comprising six IGBT switches. A PI controller is used for speed regulation, while a hysteresis current controller maintains current control within the closed-loop system. ITSCFs were introduced in phase a by varying the short-circuit ratio μ and fault resistance R_f.

Table 1. SynRM parameters

Rated power	2.2 kW
Rated voltage	220 V
Rated current	5.7 A
Rated speed	1500 rpm
N° # pole pairs	2
Moment of inertia	0.0017 Kg. m2/s
Stator resistance	1.71

To comprehensively evaluate the robustness of the proposed method, several test cases were conducted. The testing sequence was designed to:

- Validate the choice of the diagnostic indicator,
- Confirm fault-related harmonic symptoms,
- Assess detection performance under steady-state and transient conditions, and
- Analyze the effects of rotor speed and load torque on detection accuracy.

4.1. Influence of ITSCF on the Proposed Indicator ε

To validate the suitability of the proposed indicator ε, a FFT analysis was conducted on three signal sets:

- The product of measured dq-axis currents,
- The product of reference dq-axis currents,
- The difference between measured and reference dq products.

This test was performed under no-load conditions at a rated speed of 1500 rpm with an ITSCF. The results are presented in Fig. 5. Notably, the second-order harmonic amplitude in ε was 0.47 p.u., and the fourth-order harmonic measured 0.12 p.u. In contrast, the FFT of the measured dq product exhibited a second harmonic of only $9.5e^{-3}$ p.u., and the reference signal yielded $1e^{-3}$ p.u. for the same component.

These results demonstrate that the proposed indicator ε significantly amplifies the fault-related harmonics while suppressing irrelevant components masked by closed-loop control. Therefore, ε proves to be a more sensitive and effective fault indicator compared to raw dq measurements or their references.

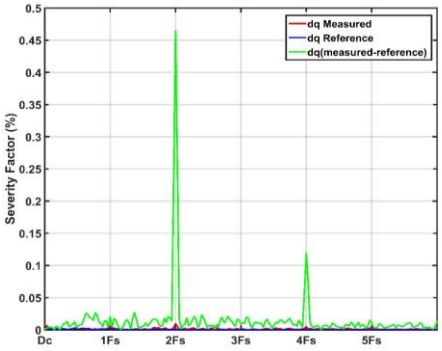

Fig. 5. FFT Results

Additionally, the FFT results confirm that ITSCFs introduce distinct second harmonic components into the dq-axis currents consistent with observations in [37] and [42].

4.2. Fault Detection in Steady State

In this test scenario, the SynRM operates at its rated speed of 1500 rpm under no-load environments. The measured phase current is approximately 5.79 A, with component currents i_d =2.7A and i_q =5.3A. An ITSCF is introduced in phase a at t =2s, with fault parameters set to R_f= 1Ω and μ=10%.

Fig. 6. illustrates the response of the system during this event. It is observed that the phase current waveform remains largely unaffected when the fault occurs. This is expected, as the closed-loop control is designed to reject external disturbances including fault conditions by interpreting them as transient perturbations. Consequently, the phase current waveform does not provide clear visual evidence of the fault.

Before t =2s, during the healthy operating phase, the amplitude of the fault current remains near zero. Right after fault inception, the amplitude sharply rises to approximately 10.5 A, indicating the onset of the ITSCF.

The normalized vector output ε_{vN} shows minor oscillations even in the healthy state, which are attributed to inverter switching frequencies and internal system noise. This baseline oscillation justifies the necessity of a fault threshold.

The extracted second harmonic I_2 is present even in the healthy state. Therefore, a threshold value is implemented to distinguish between healthy and faulty conditions. For instance, during the start-up phase (0 to 0.3 s), I_2 may briefly exceed the threshold due to transient conditions. However, this does not result in a false detection because the IC, described in Section 3.2, ensures that only sustained threshold violations trigger a FD.

The FD output as illustrated in Fig. 6 below. confirms the successful identification of the ITSCF. The detection is issued after a short delay of 0.038 s, corresponding to the duration required for the IC to satisfy the COUNT condition. This delay is essential to avoid false alarms from transient spikes.

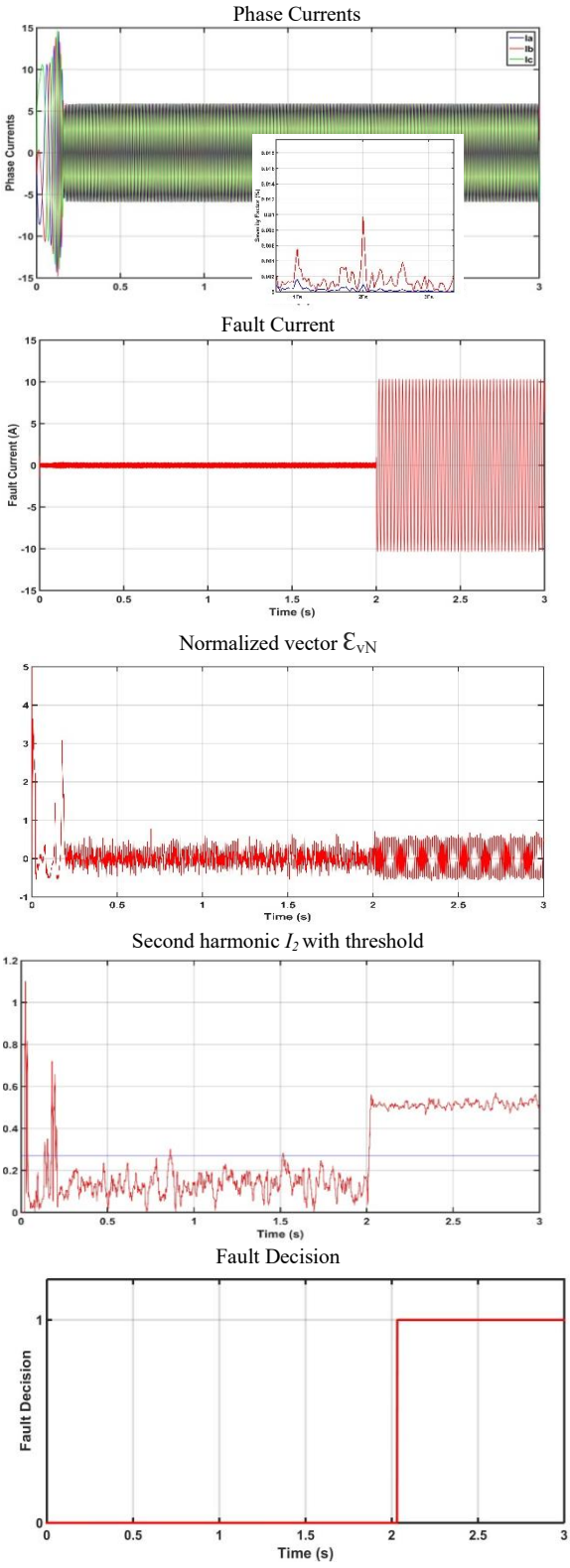

Fig. 6. The fault detection in steady-state

Unlike prior methods that rely solely on threshold crossings [37], [43], the proposed approach incorporates a time-based validation via IC, significantly enhancing detection reliability and noise immunity.

4.3. Fault Detection During Transients

To assess the robustness of proposed diagnostic technique under dynamic conditions, a transient test

was conducted. The SynRM was operated at a constant speed of 1500 rpm, while the load torque was subjected to abrupt changes:

- At: t = 0 s, T_L=7 N.m
- At: t = 1 s, T_L=14 N.m

An ITSCF was introduced at t = 2s with fault parameters R_f =1 Ω and μ=10%. The results are shown in Fig.7.

During the torque transitions, The amplitude of the phase currents varies in response to load fluctuations. However, at the moment of fault occurrence, no substantial change is observed in the phase current amplitudes demonstrating the controller's ability to mask fault effects under closed-loop operation.

The normalized indicator vector ε_{vN} reflects synchronous changes with the load torque, briefly deviating and then returning to its prior value after the transient passes. Importantly, this confirms the indicator's responsiveness to external load changes without falsely indicating a fault.

The second harmonic signal I_2, plotted in Fig.7, illustrates brief crossings of the detection threshold during transient events (e.g., at 0.8 s and 1.0 s). These short-term threshold breaches activate the IC, but the counter resets before reaching the COUNT threshold due to the temporary nature of the disturbance. Therefore, no false alarms are generated.

Upon the actual ITSCF at t = 2s, I_2 increases sharply to 0.55 p.u., and sustains this value. As a result, the IC successfully increments beyond the COUNT value, and the FD is set to 1 with a detection delay of approximately 0.038 s. Fig. 7 illustrates the described transient behaviour.

This test verifies the transient immunity of the proposed approach and its enhanced performance compared to AI-based solutions. [44] or extensive lookup tables [38] which are computationally expensive and require large datasets for various operating conditions. In contrast, this method achieves reliable detection using a single threshold and a time-validated counter mechanism.

4.4. Influence of Motor Speed and Load Torque on Diagnosis Results

This test investigates the effect of varying rotor speeds and load torque conditions on the performance of the proposed fault detection method. Simulations were carried out under two scenarios:

- Without load torque (no-load condition)
- With a constant load-torque of TL=14 N.m

In both scenarios, the rotor speed was varied across three operating points: 400 rpm, 1200 rpm, and 1500 rpm. For each speed, the fault parameters were varied using different severities:

- R_f = 10 Ω , μ = 4 %
- R_f = 1 Ω , μ = 10 %
- R_f = 0 Ω , μ = 16 %

The results are depicted in Fig. 8, with subplots (a) for no-load and (b) for loaded conditions.

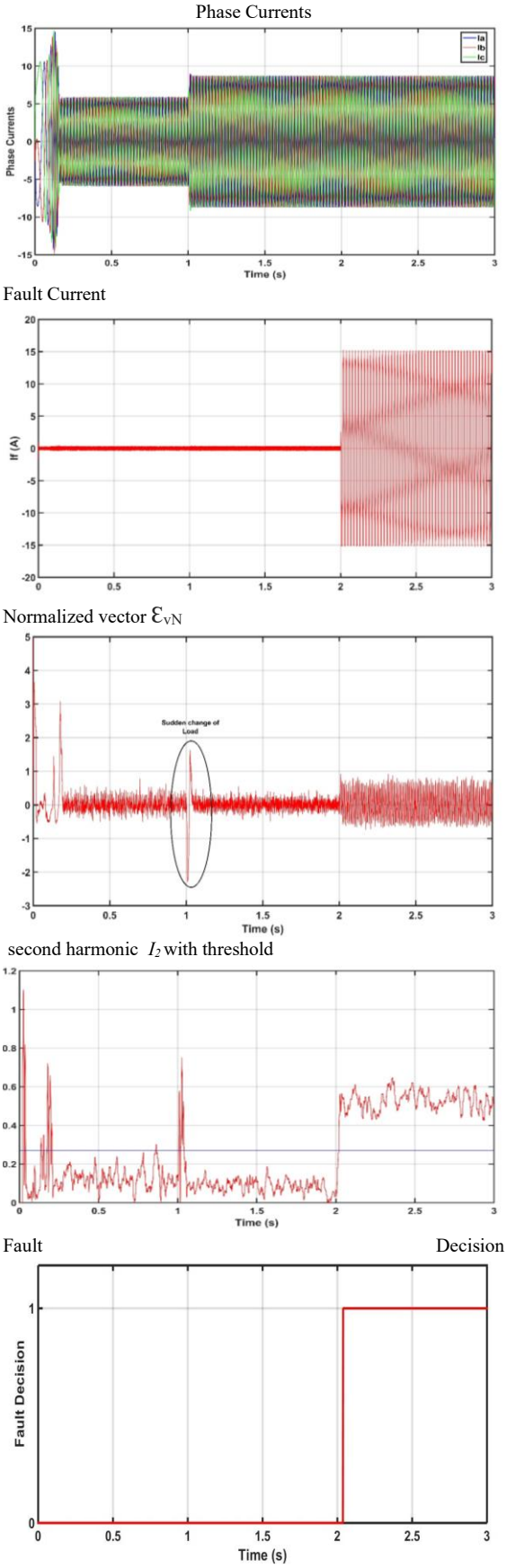

Fig. 7. The fault detection in the transients' state

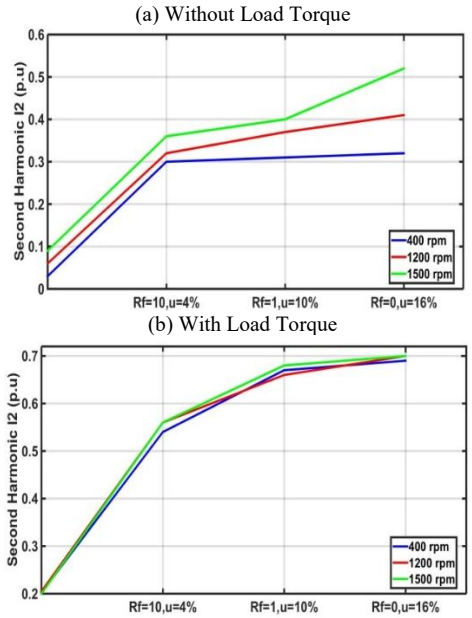

Fig. 8. Effect of rotor speed and load torque on fault detection performance.

1- No-Load Condition (Fig. 8a):

At low speed (400 rpm), the second harmonic indicator I_2 registers approximately 0.3 p.u., even for minor fault severity. As the rotor speed increases to 1200 rpm and 1500 rpm, the magnitude of I_2 increases proportionally with fault severity, confirming the indicator's sensitivity. Notably, at all tested speeds, I_2 remains above the detection threshold, validating the method's effectiveness even at low speed a traditionally challenging scenario for fault detection.

2- Loaded Condition (Fig. 8b):

Under constant torque loading (T_L=14 N.m), the results similarly show that the rotor speed has minimal influence on the magnitude of the second harmonic signal. Across all speed levels, the I_2 signal remains distinct and above the threshold for each fault severity tested.

These findings confirm that the proposed detection method is robust to variations in rotor speed and load torque. The system can reliably detect ITSCFs across a wide range of mechanical operating conditions including low-speed and no-load states, which are particularly difficult for conventional detection strategies.

5. CONCLUSION

ITSCF detection in closed-loop controlled SynRMs presents a significant challenge due to the masking effects of feedback control and the typical reliance on external sensors, high-frequency signal injection, or precise machine parameter modeling. In contrast, the method proposed in this work introduces a robust and computationally efficient solution that requires only measured and reference dq-axis currents.

A novel fault indicator was derived from the product difference between the measured and reference dq-axis currents. This indicator effectively highlights the second harmonic component introduced by ITSCFs. Unlike conventional methods, it is independent of torque sensors and model parameter estimation, and it remains reliable under a wide range of operating conditions.

The detection architecture incorporates:

- DC component removal.
- Harmonic isolation using signal modulation and filtering.
- Time-validated thresholding via an incremental counting algorithm.

Simulation results validate the method's robustness and accuracy. The proposed technique successfully detected ITSCFs during steady-state, transient load changes, and across a wide range of speeds and torque levels including traditionally difficult conditions such as low speed and no load. The reliance on a single threshold and a time-based counter eliminates the need for memory-intensive lookup tables or complex AI training models, making it ideal for real-time fault diagnosis in practical applications.

This approach offers a scalable, cost-effective, and sensor less diagnostic tool that enhances the fault tolerance and reliability of SynRM-based drive systems.

Future work will focus on extending the proposed technique beyond simulation by implementing it on embedded real-time platforms such as DSPs or FPGAs. Experimental validation using HIL setups or laboratory test benches will be conducted to evaluate detection accuracy, latency, and false alarm rates under real operating conditions. Additionally, the adaptability of the method to other machine types such as PMSMs and Interior IPMs will be investigated to assess its generalizability across motor drive technologies.

Source of funding: *The source of funding should be indicated if the article was written as part of a research project. Optionally, you can insert: This research received no external funding.*

Acknowledgment: O*ptional - this data is not required.*

Author contributions: *research concept and design, S.R., M.L., A.M.; Collection and/or assembly of data, S.R., M.L., A.M.; Data analysis and interpretation, S.R., M.L., A.M., M.A.; Writing the article, S.R., M.L., A.M.; Critical revision of the article, S.R.; Final approval of the article, J.S.*

Declaration of competing interest: *The authors declare that they have no known competing financial interests or personal relationships that could have appeared to influence the work reported in this paper.* / The author declares no conflict of interest.

REFERENCES

1. Khan A, Midha C, Lowther D. Reinforcement Learning for Topology Optimization of a Synchronous Reluctance Motor. IEEE Transactions on Magnetics.

2022;58(9):1-4. https://doi.org/10.1109/tmag.2022.3184246.
2. Tawfiq KB, Ibrahim MN, Sergeant P, Zeineldin HH, Al-Durra A, El-Saadany EF. Comparative Analysis of Reliability, Cost and Performance of Three and Five-Phase Synchronous Reluctance Machine Drive Systems with and without Permanent Magnets. IEEE Transactions on Industry Applications. 2024; 60(5): 6672–6683. https://doi.org/10.1109/tia.2024.3403807.
3. Parveen H, Sharma U, Singh B. Impacts of barrier shape on torque ripple and saliency in synchronous reluctance motor for solar water pumping. 2020 IEEE International Conference On Power Electronics, Smart Grid and Renewable Energy. 2020;1‑6. https://doi.org/10.1109/pesgre45664.2020.9070740.
4. Bao Y, Degano M, Wang S, Chuan L, Zhang H, Xu Z, Gerada C. A novel concept of ribless synchronous reluctance motor for enhanced torque capability. IEEE Transactions On Industrial Electronics. 2019; 67(4): 2553–2563. https://doi.org/10.1109/tie.2019.2914616.
5. Aladetola OD, Ouari M, Saadi Y, Mesbahi T, Boukhnifer M, Adjallah KH. Advanced torque ripple minimization of synchronous reluctance machine for electric vehicle application. Energies. 2023;16(6): 2701. https://doi.org/10.3390/en16062701.
6. Report of Large Motor Reliability Survey of Industrial and Commercial Installations, Part I. IEEE Transactions on Industry Applications. 1985;21(4): 853–864. https://doi.org/10.1109/tia.1985.349532.
7. Grubic S, Aller JM, Lu B, Habetler TG. A survey on testing and monitoring methods for stator insulation systems of low-voltage induction machines focusing on turn insulation problems. IEEE Transactions On Industrial Electronics. 2008;55(12):4127‑4136. https://doi.org/10.1109/tie.2008.2004665.
8. Faiz J, Nejadi-Koti H, Valipour Z. Comprehensive review on inter-turn fault indexes in permanent magnet motors. IET Electric Power Applications. 2017;11(1): 142‑156. https://doi.org/10.1049/iet-epa.2016.0196.
9. Zafarani M, Bostanci E, Qi Y, Goktas T, Akin B. Interturn short-circuit faults in permanent magnet synchronous machines: An extended review and comprehensive analysis. IEEE Journal Of Emerging And Selected Topics In Power Electronics. 2018;6(4): 2173‑2191. https://doi.org/10.1109/jestpe.2018.2811538.
10. Maraaba LS, Al-Hamouz ZM, Milhem AS, Abido MA. Neural network-based diagnostic tool for detecting stator inter-turn faults in line start permanent magnet synchronous motors. IEEE Access. 2019;7: 89014–89025. https://doi.org/10.1109/access.2019.2923746.
11. Singh M, Shaik AG. Incipient fault detection in stator windings of an induction motor using Stockwell transform and SVM. IEEE Transactions On Instrumentation And Measurement. 2020;69(12): 9496–9504. https://doi.org/10.1109/tim.2020.3002444
12. Lee H, Jeong H, Koo G, Ban J, Kim SW. Attention recurrent neural network-based severity estimation method for interturn short-circuit fault in permanent magnet synchronous machines. IEEE Transactions On Industrial Electronics. 2021;68(4):3445–3453. https://doi.org/10.1109/tie.2020.2978690.
13. Zhao J, Guan X, Li C, Mou Q, Chen Z. Comprehensive Evaluation of Inter-Turn Short Circuit Faults in PMSM Used for Electric Vehicles. IEEE Transactions on Intelligent Transportation Systems. 2020;22(1): 611-621. https://doi.org/10.1109/tits.2020.2987637.
14. Zhang Y, Liu G, Zhao W, Zhou H, Chen Q, Wei M. Online diagnosis of slight interturn short-circuit fault for a low-speed permanent magnet synchronous motor. IEEE Transactions on Transportation Electrification. 2020;7(1):104-113. https://doi.org/10.1109/tte.2020.2991271.
15. Hu R, Wang J, Mills A, Chong E, Sun Z. Detection and classification of turn fault and high-resistance connection fault in inverter-fed permanent magnet machines based on high-frequency signals. The Journal of Engineering 2019; 2019(17):4278-4282. https://doi.org/10.1049/joe.2018.8253.
16. Mohammed A, Melecio JI, Djurović S. Stator winding fault thermal signature monitoring and analysis by in situ FBG sensors. IEEE Transactions on industrial electronics. 2018;66(10):8082-8092. https://doi.org/10.1109/tie.2018.2883260.
17. Liu X, Miao W, Xu Q, Cao L, Liu C, Pong PWT. Inter-turn short-circuit fault detection approach for permanent magnet synchronous machines through stray magnetic field sensing. IEEE Sensors Journal. 2019;19(18):7884–7895. https://doi.org/10.1109/jsen.2019.2918018 .
18. Gurusamy V, Bostanci E, Li C, Qi Y, Akin B. A Stray Magnetic Flux Based Robust Diagnosis Method for Detection and Location of Interturn Short Circuit Fault in PMSM. IEEE Transactions on Instrumentation and Measurement. 2020;70:1‑11. https://doi.org/10.1109/tim.2020.3013128.
19. Mahmoudi A, Jlassi I, Cardoso AJM, Yahia K, Sahraoui M. Inter-turn short-circuit faults diagnosis in synchronous reluctance machines, using the Luenberger state observer and current's second-order harmonic. IEEE Transactions on Industrial Electronics. 2022;69(8):8420–8429. https://doi.org/10.1109/tie.2021.3109514.
20. Leboeuf N, Boileau T, Nahid-Mobarakeh B, Clerc G, Meibody-Tabar F. Real-time detection of interturn faults in PM drives using back-EMF estimation and residual analysis. IEEE Transactions On Industry Applications. 2011;47(6):2402–2412. https://doi.org/10.1109/tia.2011.2168929.
21. Bouchareb I, Bentounsi A, Lebaroud A. Advanced diagnosis strategy for incipient stator faults in synchronous reluctance motor. 2015 IEEE 10th International Symposium on Diagnostics for Electrical Machines, Power Electronics and Drives (SDEMPED). 2015;110–116. https://doi.org/10.1109/demped.2015.7303677.
22. Ilhem B, Amar B. Lebaroud A. Classification method for faults diagnosis in reluctance motors using Hidden Markov Models. 2014 IEEE 23rd International Symposium on Industrial Electronics (ISIE). 2014; 984–991. https://doi.org/10.1109/isie.2014.6864746.
23. Neti P, Nandi S. Performance analysis of a reluctance synchronous motor under abnormal operating conditions. Canadian Journal Of Electrical And Computer Engineering. 2008;33(2):55–61. https://doi.org/10.1109/cjece.2008.4621830.
24. Nelson AL, Chow M-Y. Characterization of coil faults in an axial flux variable reluctance PM motor. IEEE Transactions On Energy Conversion. 2002;17(3): 340–348. https://doi.org/10.1109/tec.2002.801730.
25. Navarro-Navarro A, Biot-Monterde V, Ruiz-Sarrio J E, Antonino-Daviu JA. Current-and vibration-based

detection of misalignment faults in synchronous reluctance motors. Machines. 2025;13(4):319. https://doi.org/10.3390/machines13040319.
26. Safa HH, Zarchi HA. Eccentricity fault detection in synchronous reluctance machines. Electrical Engineering. 2024;106(2):1977–1987. https://doi.org/10.1007/s00202-023-01990-5.
27. Niewiara ŁJ, Gierczyński M, Tarczewski T, Grzesiak LM. Dynamic modeling and identification of a reluctance synchronous machine parameters. Bulletin Of The Polish Academy Of Sciences Technical Sciences. 2024;72(5):151042. https://doi.org/10.24425/bpasts.2024.151042.
28. Enchev G, Milushev H, Djagarov N. Simulating a jammed rotor fault on SynRM and integrate results with machine learning. WSEAS Transactions on Systems. 2025;24:303–310. https://doi.org/10.37394/23202.2025.24.26.
29. Henriques K, Laadjal K, Cardoso AJM. Inter-turn short-circuit fault detection in synchronous reluctance machines, based on current analysis. Engineering Proceedings. 2022;24(1):23. https://doi.org/10.3390/IECMA2022-12884.
30. Heidari H, Rassõlkin A, Kallaste A, Vaimann T, Andriushchenko E, Belahcen A, Lukichev DV. A review of synchronous reluctance motor-drive advancements. Sustainability. 2021;13(2):729. https://doi.org/10.3390/su13020729.
31. Zhao M, Liu G, Wang X, Mao J, Zheng J, Zhu X. Fault-tolerant sensorless control for a 3×3-phase PMA-SynRM based on frequency adaptive extended-state-observer. IEEE Transactions On Transportation Electrification. 2024;11(1):2504‑2515. https://doi.org/10.1109/tte.2024.3423479.
32. Aliahmadi M, Mirsalim M, Milimonfared J, Moghani JS. Hybrid modeling of Joukowsky-barrier synchronous reluctance machines. IEEE Transactions on Magnetics. 2025;61(3):8100523. https://doi.org/10.1109/tmag.2025.3529489.
33. Madariaga-Cifuentes C, Gallardo C, Ruiz-Sarrio JE, Tapia JA, Antonino-Daviu JA. Comparative analysis of the effect of rotor faults in the performance of low-speed high-torque machines. Applied Sciences 2025; 15(4):1721. https://doi.org/10.3390/app15041721.
34. Zhao Y, Ren Z, Zhang L, Wang H, Ren S, Lin G, Ren L. Improved torque ripple minimization of SynRM with optimal multi-frequency harmonic current tracking. Electrical Engineering. 2025; https://doi.org/10.1007/s00202-025-03177-6.
35. Yao Y, Li Y, Yin Q. Bandpass effect and its compensation method for diagnosis in a closed-loop control system. IEEE/ASME Transactions on Mechatronics. 2020;25(3):1679–1689. https://doi.org/10.1109/tmech.2020.2982200.
36. Sun B, Wang J, He Z, Zhou H, Gu F. Fault identification for a closed-loop control system based on an improved deep neural network. Sensors 2019; 19(9):2131. https://doi.org/10.3390/s19092131.
37. Wolkiewicz M, Tarchała G, Orłowska-Kowalska T, Kowalski CT. Online stator interturn short circuits monitoring in the DFOC induction-motor drive. IEEE Transactions on Industrial Electronics. 2016;63(4): 2517–2528. https://doi.org/10.1109/tie.2016.2520902.
38. Wang B, Wang J, Griffo A, Sen B. Stator turn fault detection by second harmonic in instantaneous power for a triple-redundant fault-tolerant PM drive. IEEE Transactions on Industrial Electronics. 2018;65(9): 7279–7289. https://doi.org/10.1109/tie.2018.2793188.
39. Sun B, Wang J, He Z, Qin Y, Wang D, Zhou H. Fault detection for closed-loop control systems based on parity space transformation. IEEE Access. 2019;7: 75153–75165. https://doi.org/10.1109/access.2019.2916785.
40. Pazouki E, Islam MZ, Bonthu SSR, Choi S. Eccentricity fault detection in multiphase permanent magnet assisted synchronous reluctance motor. In 2015 IEEE International Electric Machines & Drives Conference (IEMDC). 2015;240-246. https://doi.org/10.1109/iemdc.2015.7409066.
41. Yahia K, Matos D, Estima JO, Cardoso AM. Modeling synchronous reluctance motors including saturation, iron losses and mechanical losses. In 2014 International Symposium on Power Electronics, Electrical Drives, Automation and Motion. 2014;601-606. https://doi.org/10.1109/speedam.2014.6871965.
42. Fonseca DSB, Santos CM, Cardoso AJM. Stator faults modeling and diagnostics of line-start permanent magnet synchronous motors. IEEE Transactions on Industry Applications. 2020;56(3):2590-2599. https://doi.org/10.1109/tia.2020.2979674.
43. Moon S, Jeong H, Lee H, Kim SW. Interturn short fault diagnosis in a PMSM by voltage and current residual analysis with the faulty winding model. IEEE Transactions on Energy Conversion. 2017;33(1):190-198. https://doi.org/10.1109/tec.2017.2726142.
44. Guedidi A, Laala W, Guettaf A, Arif A. Early detection and localization of stator inter turn faults based on variational mode decomposition and deep learning in induction motor. Diagnostyka 2023; 24(4): 1-13. https://doi.org/10.29354/diag/174001.

Souhaib REMHA was born in El Oued, Algeria. He obtained his B.S. and M.S. degrees in Electrical Engineering from the University of El Oued in 2011 and 2013 respectively. In 2022, he earned his Ph.D degree in Electrical Power System from Amar Telidji University, Laghouat, Algeria. Currently, he is a lecturer and researcher in the Department of Mechanical Engineering at the University of El Oued, Algeria, and a member of the UDERZA Unit, University of El Oued, Algeria. His research interests include planning and optimization problems in electrical power systems, reactive power static compensator and optimization techniques.
e-mail: remha-souhaib@univ-eloued.dz

Mosbah LAOUAMER was born in El Oued, Algeria. He received his master's degree in electrical engineering in 2012 from Echahid Hamma Lakhdar El Oued University, Algeria. In 2019, he obtained his doctorate in electrical networks from Doctor Yahia Fares Medea University, Algeria. His areas of interest include phasor measurement units, electrical networks and optimization, power factor improvement, diagnosing and monitoring faults in solar

panels, control systems, renewable energy, and the application of artificial intelligence techniques. Currently, he serves as a Lecturer B at the Department of Mechanical Engineering at the University of El Oued, Algeria, and a member of the UDERZA Unit, University of El Oued, Algeria
e-mail: laouamer-mosbah@univ-eloued.dz

Abdelkader MAHMOUDI is a lecturer and researcher in the Department of Mechanical Engineering at the University of El Oued, Algeria, and a member of the UDERZA Unit, University of El Oued, Algeria. He earned his Ph.D. in Control and Diagnosis of Electrical Systems from the Department of Electrical Engineering at the University of Biskra, Algeria. He is also a research member of the CISE—Electromechatronic Systems Research Centre, Covilhã, Portugal. His research interests include synchronous reluctance machines, model predictive control for power converters and motor drive systems, advanced control, renewable energy system control, and swarm optimization techniques. He also works on machine fault modeling, machine fault detection, and fault-tolerant control.
e-mail: abdelkader-mahmoudi@univ-eloued.dz

Mohamed ADIKA was born in El Oued, Algeria, on March 14, 2000. He received the B.S. and M.S.degrees in electrical engineering from the University of El Oued 2020 and 2022 respectively. He is currently a Ph.D. student at the Electromechanical Engineering Department and a Member in LPMRN Laboratory, University of Bordj Bou Arreridj, Algeria. His main research interests focus on the application of artificial intelligence in insulating oils.
e-mail: mohammed.adaika@univ-bba.dz

Youcef SOUFI was born in Tebessa, Algeria. He received a B.Sc. degree and Doctorate degrees from the University of Annaba, Algeria, in 1991 and 2012 respectively and a Magister degree in 1997 in Electrical Engineering from Tebessa University, Algeria. Currently, he is a Professor in the department of Electrical Engineering, Faculty of Sciences and Technology, Larbi Tebessi University, Tebessa, Algeria. His research interests include: electrical machines control, diagnostics, wind and solar energy, power electronics and drives applied to renewable and sustainable energy.
e-mail: youcef.soufi@univ-tebessa.dz